High orbital angular momentum harmonic generation

J. Vieira, R.M.G.M. Trines, E.P. Alves, R.A. Fonseca, J.T. Mendonça, R. Bingham, P. Norreys, and L.O. Silva

Published version information:

Citation: Vieira, J et al. "High orbital angular momentum harmonic generation." Physical Review Letters, 117, no. 26 (2016): 265001.

doi: 10.1103/PhysRevLett.117.265001

High Orbital Angular Momentum Harmonic Generation

J. Vieira,[1] R. M. G. M. Trines,[2] E. P. Alves,[1] R. A. Fonseca,[1,3] J. T. Mendonça,[1] R. Bingham,[2] P. Norreys,[2,4] and L. O. Silva[1]
[1]GoLP/Instituto de Plasmas e Fusão Nuclear, Instituto Superior Técnico, Universidade de Lisboa, Lisbon, Portugal
[2]Central Laser Facility, STFC Rutherford Appleton Laboratory, Didcot, OX11 0QX, United Kingdom
[3]DCTI/ISCTE Lisbon University Institute, 1649-026 Lisbon, Portugal
[4]Department of Physics, University of Oxford, Oxford OX1 3PU, United Kingdom
(Received 24 June 2016; revised manuscript received 17 September 2016; published 20 December 2016)

We identify and explore a high orbital angular momentum (OAM) harmonics generation and amplification mechanism that manipulates the OAM independently of any other laser property, by preserving the initial laser wavelength, through stimulated Raman backscattering in a plasma. The high OAM harmonics spectra can extend at least up to the limiting value imposed by the paraxial approximation. We show with theory and particle-in-cell simulations that the orders of the OAM harmonics can be tuned according to a selection rule that depends on the initial OAM of the interacting waves. We illustrate the high OAM harmonics generation in a plasma using several examples including the generation of prime OAM harmonics. The process can also be realized in any nonlinear optical Kerr media supporting three-wave interactions.

DOI: 10.1103/PhysRevLett.117.265001

Unlike cylindrically symmetrical wave fronts, which have an intensity maximum on-axis and nearly flat wave fronts, OAM lasers have doughnut intensity profiles and helical wave fronts. Since the seminal paper by Allen *et al.* [1], these unique properties have led to many scientific and technological advances. Experiments demonstrated the generation of entangled photons with OAM, opening new directions in quantum computing [2]. The OAM also promises to greatly enhance optical communications [3]. It plays a pivotal role in super-resolution microscopy [4], allows for new kinds of optical tweezers [5], and it might be even used as a diagnostic for rotating black holes [6]. From a fundamental perspective, all of these important contributions have only been possible because the OAM is a fundamental property of light, which can be controlled as an independent degree of freedom.

There are optical processes, such as high harmonic generation [7] (HHG), where independent OAM and frequency manipulations are not allowed. Because energy and momentum are conserved, it is natural to assume that the nth harmonic of a laser pulse with initial OAM level ℓ and photon energy $\hbar\omega$ has OAM $n\ell$ and energy $n\hbar\omega$. Much effort has been dedicated to demonstrate this hypothesis. Apart from an exceptional result that seemed to break this assumption [8], experiments [9–11] and theoretical modeling [12–14] confirmed energy and momentum conservation in HHG, which then became the dominant view of HHG using vortex lasers.

In contrast, in this Letter we identify a Raman scattering process to create high OAM harmonics that preserves the laser frequency and total angular momentum, thereby manipulating the OAM independently of any other laser property. An interesting path to produce lasers with very high OAM levels, in which the OAM and frequency harmonics are still coupled, has been recently suggested [9]. As we will show, however, only by independently controlling the OAM and laser frequency can the potential of OAM for several applications (e.g., super-resolution microscopy) become fully realized.

We consider a three-wave interaction mechanism, stimulated Raman backscattering, in a plasma [15–22]. Raman backscattering has been investigated in the frame of one-dimensional physical models [23,24], focusing on energy flows between the intervening waves. As an application, we recently showed that Raman backscattering can amplify seed pulses with a single OAM level to the required intensities to explore relativistic laser-plasma interactions [21,25–27]—by using a counter-propagating long pump laser that also contains a single OAM mode [28]. Here we demonstrate that three-wave interactions can also be used to manipulate, with an unprecedented degree of controllability, the three-dimensional spatial-temporal laser pulse structure. Specifically, we show that the seed will gain high OAM harmonics while preserving its carrier frequency if the pump contains several modes with different OAM levels [Fig. 1(a)]. The OAM harmonics extend, at least, up to the paraxial limit. These results demonstrate that the scope of stimulated Raman backscattering and, more generally, three-wave processes, goes beyond laser amplification by enabling an unexplored type of spatial-temporal control that has never been considered. Because the technique controls the OAM as an independent degree of freedom, a combination of the conventional HHG scheme and the Raman scheme opens the way for producing lasers with extremely high OAM levels, and, simultaneously, very high photon frequencies.

The order of the high OAM harmonics follows a simple algebraic expression only involving the initial OAM of the intervening lasers, being given by $\ell = \ell_1 + m\Delta\ell$, where

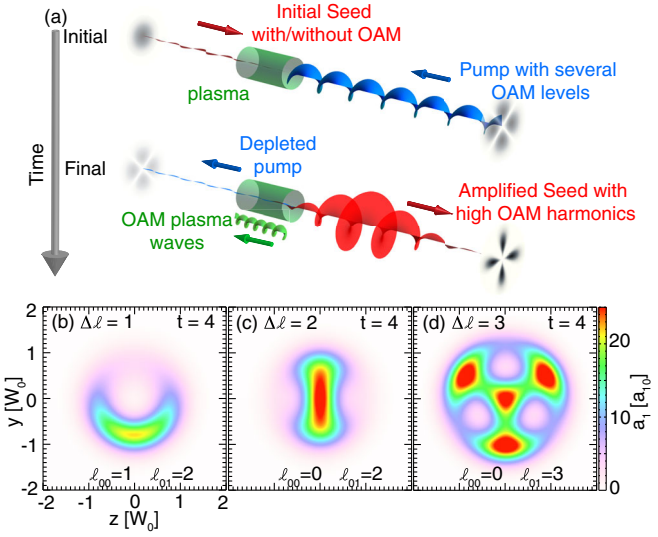

FIG. 1. (a) Illustration of the high OAM harmonics generation mechanism in stimulated Raman scattering. The high OAM harmonics are formed in a seed beam (red) after the interaction with a pump beam with several OAM modes in the nonlinear medium (plasma). (b)–(d) Transverse field profile of an initially Gaussian laser pulse seed after interacting with a counter-propagating pump. Initially, $a_{00} = a_{01} = a_1 = 1.0$ and time t is normalized to $t = \sqrt{\alpha\omega_p/\omega_1}$. (b)–(d) show the seed pulse after interacting with a pump with $\Delta\ell = 1$ (b), $\Delta\ell = 2$ (c), and $\Delta\ell = 3$, (d) respectively.

ℓ_1 is the initial seed OAM and $\Delta\ell = \ell_{00} - \ell_{01}$ is the OAM difference between two pump modes. The high OAM harmonics result from the angular momentum cascading from the modes with lower OAM to the modes with higher OAM. This is an unexpected and unexplored behavior, which is profoundly related to the role of the plasma wave as a spiral phase element. Thus, similar mechanisms are expected when dealing with waves or oscillations in other nonlinear media, e.g., phonons or molecular vibrations. We confirm the analytical predictions numerically through *ab initio* three-dimensional OSIRIS simulations [29,30]. OSIRIS employs the particle-in-cell (PIC) technique, taking into account the kinetic plasma response at the single particle level, in the presence of the external and self-consistently generated electromagnetic fields and without any physical approximations to the extent where quantum effects can be neglected.

In the small signal regime, valid when the amplitude of the seed is much smaller than that of the pump, the evolution of the seed envelope a_1 is given by [28]

$$\mathbf{a}_1(t) = \left(\mathbf{a}_1(t=0)\cdot\frac{\mathbf{a}_0^*}{|\mathbf{a}_0|}\right)\frac{\mathbf{a}_0}{|\mathbf{a}_0|}\cosh(\Gamma t), \tag{1}$$

$$\Gamma^2 = \frac{e^2k_p^2\omega_p^2}{8\omega_0\omega_1 m_e^2}|\mathbf{a}_0|^2, \tag{2}$$

where a_0 is the envelope of the pump, ω_p, ω_0, and ω_1 are the frequencies of the plasma wave, pump, and seed lasers, respectively (corresponding wavelengths are given by λ_p, λ_0 and, λ_1, respectively). In addition, e and m_e are the electron charge and mass, $k_pc = \omega_0(2 - \omega_p/\omega_0 - \omega_p^2/\omega_0^2) \sim 2\omega_0 - \omega_p$ is the plasma wave number, and c is the speed of light. Equations (1) and (2) are similar to the solutions of other three-wave interaction processes in the small signal regime, such as frequency sum or difference generation for instance. Equations (1) and (2) also describe stimulated Raman backscattering of lasers with arbitrary polarizations (although seed and pump need to have nonorthogonal polarization components for Raman to occur) and arbitrary transverse field envelopes profiles. Here we focus on the scenario where the lasers are linearly polarized in the same direction, and where the pump laser contains several Laguerre Gaussian modes.

Unlike lasers described by a single OAM level, the time-averaged intensity envelope of a laser containing several OAM levels is no longer cylindrically symmetric. Consider, for instance, the superposition between two modes with ℓ_{00} and ℓ_{01} each with peak vector potential given by a_{00} and a_{01}. The corresponding transverse intensity envelope $[I_0(\mathbf{r}) \propto a_0a_0^*]$, given by $I \propto a_{00}^2 + a_{01}^2 + 2a_{00}a_{01}\cos[(\ell_{00} - \ell_{01})\phi]$, contains a cylindrically symmetric term $(a_{00}^2 + a_{01}^2)$, corresponding to the sum of the intensity envelopes of each individual Laguerre-Gaussian component, and a noncylindrically symmetric component $(2a_{00}a_{01}\cos[(\ell_{00} - \ell_{01})\phi])$ that corresponds to the beating of the two Laguerre-Gaussian modes. This analysis shows that noncylindrically symmetric pump lasers resulting from the combination of several OAM modes change key properties of stimulated Raman backscattering because the growth rate, given by Eq. (2), now depends on ϕ. The ϕ dependent growth rate can significantly reshape the intensity of the seed, as shown in Figs. 1(b)–(d). Figures 1(b)–(d) show the final intensity profile of an initially Gaussian seed pulse $(\ell_1 = 0)$ using a pump that is a superposition of OAM states according to Eqs. (1) and (2). The seed transverse envelope develops evenly spaced lobes at well-defined locations along the azimuthal ϕ direction. The number of lobes corresponds to $\Delta\ell \equiv \ell_{00} - \ell_{01}$. For $\Delta\ell = 1$, a single lobe appears [Fig. 1(b)]. When $\Delta\ell = 2$, two lobules are formed spaced by $\Delta\phi = \pi$ [Fig. 1(c)], and when $\Delta\ell = 3$ there are three lobules separated by $\Delta\phi = 2\pi/3$ [Fig. 1(d)]. We note that a_{00} and a_{01} (and a_1) are the local, radius dependent amplitudes of each mode.

The laser envelopes shown in Figs. 1(b)–(d) contain high OAM harmonics. High OAM harmonics generation in stimulated Raman scattering results directly from the conservation of OAM. Initially, the seed is described by a single Laguerre-Gaussian mode with ℓ_1, and the pump described by two OAM modes ℓ_{00} and ℓ_{01}. This seed mode beats with each pump mode exciting a Langmuir plasma wave. In order to conserve angular momentum, the two modes in the plasma have $\ell_{00} - \ell_1$ and $\ell_{01} - \ell_1$; i.e., the modes in the plasma absorb the OAM difference between

every pump mode and the seed. The beating of these two plasma modes with the pump is at the onset of the cascading mechanism that leads to the high OAM harmonic generation. The pump ℓ_{00} beating with the plasma $\ell_{01}-\ell_1$ preserves the initial OAM if a new seed component appears with $\ell_1+\Delta\ell$ ($\Delta\ell\equiv\ell_{00}-\ell_{01}$). Similarly, the pump ℓ_{01} beating with the plasma $\ell_{00}-\ell_1$ preserves the OAM if another seed mode component grows with $\ell_1-\Delta\ell$. These are the first OAM sideband harmonics growing in the seed. Each of these sidebands will beat with the pump, adding new higher-order OAM sidebands to the plasma wave. In general, each new mode in the plasma wave continues to interact with every pump mode, generating higher OAM seed modes $\ell_1\pm m\Delta\ell$, with integer m. The high OAM harmonics then appear because the plasma wave is in a superposition of OAM states. This unexpected behavior, due to the wavelike plasma response, has no counterpart in other optical devices such as spiral wave plates.

An analytical theory for the evolution of each seed OAM harmonic supports this qualitative interpretation. Instead of taking an azimuthal Fourier transform of Eq. (1), which cannot be determined analytically, we start with the general differential equation that describes the evolution of the linearly polarized seed in the small signal regime, $d_t^2 a_1=\alpha a_1(a_0 a_0^*)=\alpha a_1[a_{00}^2+a_{01}^2+2a_{00}a_{01}\cos(\Delta\ell\phi)]$, where $d_t^2=d^2/dt^2$ and $\alpha=(e^2\omega_p^3/8m_e^2c^2\omega_1)=\Gamma/|\mathbf{a_0}|$. Instead of focusing in the amplification properties of stimulated Raman backscattering, we describe, theoretically, the evolution of the inner three-dimensional spatial-temporal OAM structure of the seed. The evolution of the amplitude of each OAM component, $f_m=(1/2\pi)\int_0^{2\pi}a_1\exp(-im\phi)d\phi$, can be readily obtained by multiplying the equation by $(1/2\pi)\exp(-im\phi)$ and then by integrating over ϕ. This procedure, presented in detail in the Supplemental Material [31], leads to the following differential equation for the evolution of each seed mode:

$$\frac{d^2 f_m}{dt^2}=\frac{e^2\omega_p^3}{8m_e^2c^2\omega_1}[(a_{00}^2+a_{01}^2)f_m+a_{00}a_{01}(f_{m+\Delta\ell}+f_{m-\Delta\ell})]. \tag{3}$$

Equation (3) predicts the generation of high OAM harmonics. Unlike in conventional high (frequency) harmonic generation, however, the frequency of the laser remains unchanged in Eq. (3). According to Eq. (3), each mode m grows from of its (unstable) coupling with the plasma and the pump [first term on the left-hand side of Eq. (3)]. In addition, each mode is also driven by its closest sideband mode with $\ell=m\pm\Delta\ell$ [second term on the left-hand side of Eq. (3)]. We can clarify the predictions of Eq. (3) by distinguishing three cases: At early times the fundamental mode ℓ_1 is driven by the first term on the right-hand side (rhs) of Eq. (3) even if the second term is not immediately available for these modes. Then, sideband modes at $\ell_1\pm|m|\Delta\ell$ are created and amplified once the second term on the rhs of Eq. (3) appears because the first term is not initially available. The modes between $\ell_1\pm|m|\Delta\ell$ and $\ell_1\pm|m\pm1|\Delta\ell$ will never grow since neither the first or the second term on the rhs of Eq. (3) will ever be available.

The evolution of the high OAM harmonics at sufficiently early times, for which the higher OAM sidebands are driven by their closest neighbor OAM mode, is

$$a_1^{\ell_1\pm|m|\Delta\ell}(t)=a_1\left(\frac{a_{00}a_{01}}{a_{00}^2+a_{01}^2}\right)^{|m|}\left(\cosh(\Gamma t)-\sum_{i=0}^{|m|-1}\frac{(\Gamma t)^{2i}}{(2i)!}\right), \tag{4}$$

where $\Gamma^2=e^2k_p^2\omega_p^2/(8\omega_0\omega_1 m_e^2)(a_{00}^2+a_{01}^2)$. Figure 2 compares the numerical solution to Eq. (1), valid in the small signal approximation, with the analytical solution of Eq. (3) given by Eq. (4), which considers that the growth of each mode is only driven by the amplitude of the preceding sideband. The comparison assumed spatially uniform a_{00}, a_{01}, and a_1. The agreement is excellent at early times and holds for different pump OAM compositions $\Delta\ell$ as long as the growth of the OAM harmonics are driven by their closest neighbors. A subsequent approximation to Eq. (4) can be obtained by retaining the leading order term of the factor between the big brackets in Eq. (4):

$$a_1^{\ell\pm|m|\Delta\ell}\simeq a_1\left(\frac{a_{00}a_{01}}{a_{00}^2+a_{01}^2}\right)^{|m|}\frac{(\Gamma t)^{2|m|}}{(2m)!} \tag{5}$$

Figure 2 compares the numerical solution of Eq. (1) and the analytical solution given by Eq. (5). The agreement is very good for $m\gtrsim 4$.

Equations (3) and (4) predict OAM harmonic generation for arbitrarily high OAM orders. Our theory, however, is not valid beyond the paraxial approximation, which can be employed as long as the longitudinal laser wave number, $k_\parallel$, is much higher than the transverse laser wave number. This assumption no longer holds when the azimutal wave number $k_\phi\sim\ell/r_0$ becomes of the same order of $k_\parallel$, i.e., when $|k_\phi|\simeq k_\parallel$ ($r_0=w_0\sqrt{\ell}$ is the distance from the origin to the radius of maximum intensity, w_0 is the laser spot size). Since $k_\parallel=2\pi/\lambda_0$, the high OAM harmonics

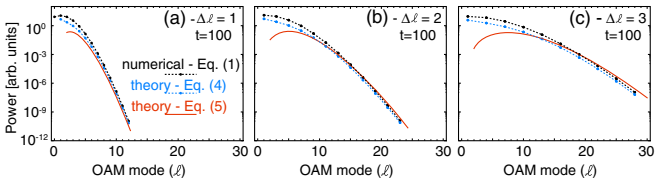

FIG. 2. Comparison between the numerical [thick dashed black, Eq. (1)] and theoretical prediction [dashed blue, Eq. (4); solid red, Eq. (5)] for the generation of the high OAM harmonics Fourier power spectra. Calculations assumed $a_{00}=a_{01}=0.1$ and $a_1=0.01$, and normalized growth rate $\Gamma=|\mathbf{a_0}|$, and time is normalized to $\sqrt{\alpha\omega_p/\omega_1}$. Initially the seed pulse has $\ell_1=1$. The pump has $\Delta\ell=1$ in (a); $\Delta\ell=2$ in (b) and $\Delta\ell=3$ in (c).

generation will differ from the predictions of Eq. (1) when $|\ell| \simeq r_0\omega_1/c \simeq 2\pi r_0/\lambda_1$ (additional arguments for the maximum ℓ allowed by the paraxial approximation provided in the Supplemental Material [31]).

The high OAM harmonic orders are produced according to the simple algebraic relation $\ell_1 + m\Delta\ell$. All OAM harmonics will be then generated when $\Delta\ell = 1$. Figures 1(b) and 2(a) illustrate this scenario. Even harmonics appear when $\Delta\ell = 2$ with even ℓ_1 [Figs. 1(c) and 2(b)]. When ℓ_1 is odd, then odd OAM harmonics appear instead. To illustrate high OAM harmonics generation, we have also performed three-dimensional OSIRIS PIC simulations [29,30] (simulation parameters provided in the Supplemental Material [31]). The waists of the intervening OAM modes were chosen to ensure significant overlap at the start of the interaction. Since the interaction length is much shorter than the Rayleigh lengths, there is significant overlap during propagation. Figure 3 shows the seed electric field using $\Delta\ell = 1$ [Figs. 3(a) and 3(b)] and $\Delta\ell = 2$ [Figs. 3(c) and (d)] in the pump. The initial OAM of the Gaussian seed ($\ell_1 = 0$) does not change because the amplitude of each pair of positive and negative sideband harmonic is the same. Thus, the initially Gaussian ($\ell_1 = 0$) seed pulse phase fronts remain flat during the process, as shown in Figs. 3(a) and 3(c). For $\ell_1 \neq 0$, the phase fronts would be twisted. Each positive and negative high OAM harmonic creates an azimutal beat-wave pattern that modulates the initial seed pulse transverse field profile. These transverse modulations, shown in Figs. 3(b) and 3(d) confirm the growth of positive and negative OAM harmonics. They are also very similar to the theoretical predictions shown in Figs. 1(b) and (c), supporting the validity of the theoretical model.

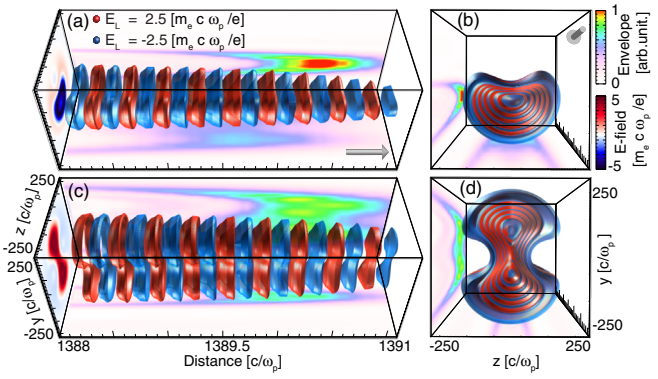

FIG. 3. PIC simulation results showing the seed pulse electric field containing high OAM harmonics while it is still in the plasma (not shown). The seed pulse is Gaussian. The pump has $\Delta\ell = 1$ in (a),(b) and $\Delta\ell = 2$ in (c),(d). Seed electric field (E) isosurfaces of the seed pulse shown in blue ($E < 0$) and in red ($E > 0$). The x-y and x-z projections show the central envelope of the seed electric field. The y-z projection shows the laser electric field at a longitudinal position (x) close to the laser peak intensity. The arrows indicate the laser propagation direction. Distances are in units of $1c/\omega_p = 2.5\ \mu$m.

Figure 4 shows the Fourier coefficients from the PIC simulations using several seed and pump OAM combinations. Figure 4(a) and the thick red line in Fig. 4(b), which show the Fourier coefficients of the laser in Fig. 3, confirm the generation of all OAM harmonics [Fig. 4(a)] and even modes only [Fig. 4(b), thick red line], in agreement with theory. Figure 4(b) (thin blue line) also shows the generation of the odd OAM harmonics using $\ell_1 = 1$.

To further demonstrate the high controllability of the process, we provide an all-optical demonstration of the Green-Tao prime number theorem [35]. The Green-Tao theorem states that for every natural number k, there exist natural numbers $a(k) + b(k)$ such that the numbers in the sequence $a(k), a(k) + b(k), a(k) + 2b(k), \ldots, a(k) + (k-1)b(k)$ are all prime. This arithmetic progression corresponds to the OAM levels produced during high OAM harmonic generation with $a = \ell_1$ and $b = \Delta\ell$. Figure 4(c) shows the generation of prime numbers with $\Delta\ell = 4$ and $\ell_1 = 3$, providing (positive) primes up to 11. Theoretical predictions are very accurate for the positive OAM sideband generation. The numerical diagnostic used to decode the seed OAM harmonics does not fully discern between positive and negative OAMs. As a result, Fig. 4(c) shows the reflection of the positive OAM sidebands in the negative OAM spectral region. Figure 4(d) shows a more demanding scenario, generating primes smaller than 29, using $\Delta\ell = 6$ and $\ell_1 = -1$. In fact, Fig. 4 shows OAM levels all prime except for -1 and -25 (if we take the modulus), giving a total of 8 OAM prime harmonics. We note that the laser spot sizes were adjusted to maximize the overlap between the seed and pump.

We conclude by outlining a scheme that could boost current super-resolution microscopy techniques [4], while also highlighting the importance of controlling the OAM as an independent degree of freedom. Consider a petal laser pulse consisting of two Laguerre-Gaussian modes with OAM levels $+\ell$ and $-\ell$. The distance between consecutive

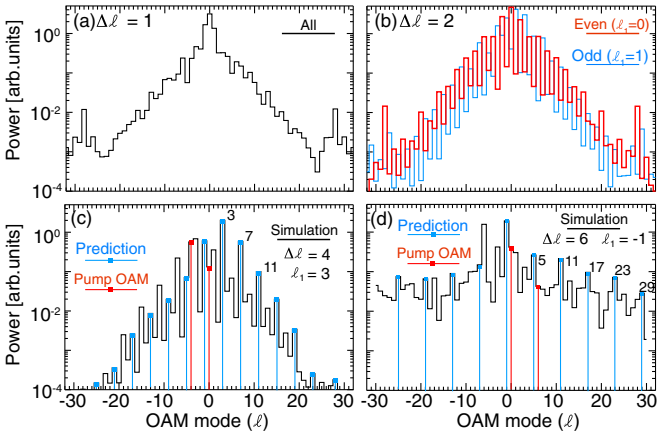

FIG. 4. PIC simulation results showing high OAM harmonics spectra at $z = 1386.71c/\omega_p$ (a), $z = 1389.01c/\omega_p$ (b), $z = 1450.14c/\omega_p$ (c), and $z = 1443.16c/\omega_p$ (d).

intensity maxima is $d = 2\pi r_0/\ell$, where $r_0 = w_0\sqrt{\ell}$ is the radial distance from the axis at which the intensity is maximum. The distance d is also a figure for the resolution of an imaging system based on these beams. Simple arithmetic calculations show that d decreases to $d_{\mathrm{HHG}} = 2\pi w_0/\sqrt{n\ell}$ for the nth harmonic in conventional HHG. Thus, resolution increases by $\sqrt{n}$. Combining conventional HHG with the Raman scheme can reduce d even more, to, at least, $d_{\mathrm{Raman-HHG}} = (w_0/\lambda_0)[1/\sqrt{\ell}](1/n)$ within the paraxial approximation, at least a factor of $\sqrt{n}$ smaller than d_{HHG}. The high OAM harmonics could be detected experimentally by using computer generated holograms (as in [2]) and will become spatially separated in vacuum due to the differences in their group velocities [36]. The mechanism can be generalized for other complete sets of solutions of the paraxial wave equations, such as the Hermite-Gaussian basis. Because OAM harmonics generation is a result of the wavelike nature of the plasma wave as an optical element, our work may be lead to new types of spiral phase elements capable of enhancing OAM manipulation.

The authors acknowledge fruitful discussions with Dr. Fabien Quéré. We acknowledge PRACE for access to resources on the Fermi supercomputer (Italy). This work was supported by the European Research Council through the inPairs project Grant Agreement No. 695088 and by the EU (EUPRAXIA Grant Agreement No. 653782). We acknowledge PRACE for access to resources on the Fermi supercomputer (Italy).

[1] L. Allen, M. W. Beijersbergen, R. J. C. Spreeuw, and J. P. Woerdman, Phys. Rev. A **45**, 8185 (1992).
[2] A. Mair, A. Vaziri, G. Weihs, and A. Zeilinger, Nature (London) **412**, 313 (2001).
[3] J. Wang *et al.*, Nat. Photonics **6**, 488 (2012).
[4] S. Hell and J. Wichmann, Opt. Lett. **19**, 780 (1994).
[5] M. Padgett, Proc. R. Soc. A **470**, 20140633 (2014).
[6] F. Tamburini, B. Thidé, G. Molina-Terriza, and G. Anzolin, Nat. Phys. **7**, 195 (2011).
[7] P. A. Franken, A. E. Hill, C. W. Peters, and G. Weinreich, Phys. Rev. Lett. **7**, 118 (1961).
[8] M. Zurch, C. Kern, P. Hansinger, A. Dreischuh, and Ch. Spielmann, Nat. Phys. **8**, 743 (2012).
[9] G. Gariepy, J. Leach, K. T. Kim, T. J. Hammond, E. Frumker, R. W. Boyd, and P. B. Corkum, Phys. Rev. Lett. **113**, 153901 (2014).
[10] D. Gauthier *et al.*, arXiv:1610.08025.
[11] J. Courtial, K. Dholakia, L. Allen, and M. J. Padgett, Phys. Rev. A **56**, 4193 (1997).
[12] J. T. Mendonça and J. Vieira, Phys. Plasmas **22**, 123106 (2015).
[13] D. F. Gordon, B. Hafizi, and A. Ting, Opt. Lett. **34**, 3280 (2009).
[14] H. Sobhani, H. Rooholamininejad, and A. Bahrampour, J. Phys. D **49**, 295107 (2016).
[15] D. W. Forslund, J. M. Kindel, and E. L. Lindman, Phys. Fluids **18**, 1002 (1975).
[16] G. Shvets, N. J. Fisch, A. Pukhov, and J. Meyer-ter-Vehn, Phys. Rev. Lett. **81**, 4879 (1998).
[17] V. M. Malkin, G. Shvets, and N. J. Fisch, Phys. Rev. Lett. **82**, 4448 (1999).
[18] J. Ren, W. Cheng, S. Li, and S. Suckewer, Nat. Phys. **3**, 732 (2007).
[19] R. M. G. M. Trines, F. Fiúza, R. Bingham, R. A. Fonseca, L. O. Silva, R. A. Cairns, and P. A. Norreys, Nat. Phys. **7**, 87 (2011).
[20] R. M. G. M. Trines, F. Fiuza, R. Bingham, R. A. Fonseca, L. O. Silva, R. A. Cairns, and P. A. Norreys, Phys. Rev. Lett. **107**, 105002 (2011).
[21] J. T. Mendonça, B. Thidé, and H. Then, Phys. Rev. Lett. **102**, 185005 (2009).
[22] G. M. Fraiman, N. A. Yampolsky, V. M. Malkin, and N. J. Fisch, Phys. Plasmas **9**, 3617 (2002).
[23] D. S. Clark and N. J. Fisch, Phys. Plasmas **10**, 3363 (2003).
[24] R. L. Berger, D. S. Clark, A. A. Solodov, E. J. Valeo, and N. J. Fisch, Phys. Plasmas **11**, 1931 (2004).
[25] J. T. Mendonça and J. Vieira, Phys. Plasmas **21**, 033107 (2014).
[26] J. Vieira and J. T. Mendonça, Phys. Rev. Lett. **112**, 215001 (2014).
[27] C. Brabetz, S. Busold, T. Cowan, O. Deppert, D. Jahn, O. Kester, M. Roth, D. Schumacher, and V. Bagnoud, Phys. Plasmas **22**, 013105 (2015).
[28] J. Vieira, R. M. G. M. Trines, E. P. Alves, R. A. Fonseca, J. T. Mendonça, R. Bingham, P. Norreys, and L. O. Silva, Nat. Commun. **7**, 10371 (2016).
[29] R. A. Fonseca *et al.*, *Lecture Notes Comp. Science* (Springer, Berlin/Heidelberg, 2002), Vol. 2331/2002.
[30] R. A. Fonseca, J. Vieira, F. Fiuza, A. Davidson, F. S. Tsung, W. B. Mori, and L. O. Silva, Plasma Phys. Controlled Fusion **55**, 124011 (2013).
[31] See Supplemental Material at http://link.aps.org/supplemental/10.1103/PhysRevLett.117.265001, which includes Refs. [15,29,31,33–35], for a description of the analytical model and physical picture of the high OAM harmonics generation mechanism.
[32] P. Mardahl *et al.*, Bull. Am. Phys. Soc. **46**, DPP2001, KP1.108 (2001).
[33] P. Mardahl, Ph.D. thesis, University of California, Berkeley, 2001.
[34] R. Zambrini, L. C. Thomson, S. M. Barnett, and M. Padgett, J. Mod. Opt. **52**, 1135 (2005).
[35] B. Green and T. Tao, Ann. Math. **167**, 481 (2008).
[36] D. Giovannini, J. Romero, V. Potoček, G. Ferenczi, F. Speirits, S. M. Barnett, D. Faccio, and M. J. Padgett, Science **347**, 857 (2015).

STIMULATED RAMAN SCATTERING

For the sake of completeness, we review here the starting point for describing stimulated Raman scattering in plasmas. In a plasma, Raman backscattering occurs when a long laser (pump), with frequency and wavenumber (ω_0, k_0), decays into a Langmuir plasma wave (ω_p, k_p) and into a counter propagating scattered light wave (seed) with (ω_1, k_1) [1]. The frequency and wavenumber of the pump, seed and plasma wave are related through the energy and momentum conservation relations, which are given by $\omega_0 = \omega_1 + \omega_p$ and $k_0 = k_p - k_1$, where $\omega_p = \sqrt{n_0 e^2/m_e\epsilon_0} = ck_p$ is the plasma frequency, k_p the plasma wavenumber, ϵ_0 is the vacuum permittivity, e is the elementary charge, m_e the mass of the electron and where n_0 is the background plasma density. These matching conditions ensure energy conservation (frequency matching) and momentum conservation (wavenumber matching), and can be obtained by assuming that the pump, the seed and the plasma wave are well described as plane waves.

When light has orbital angular momentum, the frequency and wavenumber matching conditions need to be supplemented by an additional relation ensuring conservation of orbital angular momentum. If the orbital angular momentum of the pump, seed and plasma wave is given by ℓ_0, ℓ_1, and ℓ_p respectively, then orbital angular momentum conservation requires that $\ell_0 = \ell_p - \ell_1$ [2]. In order to understand stimulated Raman backscattering of lasers in a superposition of OAM modes we employ a generalised theory valid for arbitrary laser transverse profiles. We consider that pump and seed have a complex field amplitude given by $\mathbf{a}_{0,1}(\mathbf{r})\exp\left[ik_{0,1}z - \omega_{0,1}t\right] + c.c.$ and that the amplitude of the resulting plasma wave density perturbation is given by $\delta n(\mathbf{r})\exp\left[ik_p z - \omega_p t\right] + c.c.$, where $\mathbf{r}$ is the position. The slowly varying envelopes profiles of the pump and the seed lasers ($\mathbf{a}_{0,1}$) that propagate along the longitudinal z direction, and the slowly varying envelope of the plasma wave (δn), obey the paraxial wave equation, for which the system can be reduced to the one-dimensional stimulated Raman scattering equations [2]. In these conditions the temporal evolution of the stimulated Raman backscattering instability is given by the following coupled set of first-order differential equations:

$$\frac{\mathrm{d}\mathbf{a}_0}{\mathrm{d}t} = -i(\omega_p^2/2\omega_0)\delta n\mathbf{a}_1 \tag{1}$$

$$\frac{\mathrm{d}\mathbf{a}_1}{\mathrm{d}t} = -i(\omega_p^2/2\omega_1)\delta n^* \mathbf{a}_0 \tag{2}$$

$$\frac{\mathrm{d}\delta n}{\mathrm{d}t} = -i(e^2 k_p^2/4m_e^2\omega_p)\mathbf{a}_1^* \cdot \mathbf{a}_0 \tag{3}$$

These equations are formally identical to parametric amplification in nonlinear media with Kerr nonlinearity. The evolution of the pump can be neglected in the small signal regime where $\mathbf{a}_0 \gg \mathbf{a}_1$, for which the seed evolves according to Eq. (1) in the main manuscript.

AMPLITUDE OF THE OAM HARMONICS

In order to derive analytical formulas for the amplitudes of the OAM harmonics we consider neglect the pump depletion, such that the pump laser pulse is non-evolving. We also assume linearly polarised laser pulses. We then take the derivative of Eq. (2) with respect to time, and insert Eq. (3) in the resulting expression, yielding:

$$\frac{\mathrm{d}^2 a_1}{\mathrm{d}t^2} = \frac{e^2 k_p^2}{8\omega_1 m_e^2} a_1 |a_0|^2. \tag{4}$$

In order to generate the OAM harmonics generation the pump needs to be a combination of modes with different OAM levels. If we assume that the pump has two OAM modes ℓ_{00} and ℓ_{01}, each with amplitudes a_{00} and a_{01}, then the term $|a_0|^2$ in Eq. (4) becomes:

$$|a_0|^2 = a_{00}^2 + a_{01}^2 + a_{00}a_{01}\left[\exp\left(i\Delta\ell\phi\right) + \exp\left(-i\Delta\ell\phi\right)\right], \tag{5}$$

where $\Delta\ell = \ell_{00} - \ell_{01}$.

Inserting Eq. (5) into Eq. (4) gives:

$$\frac{\mathrm{d}^2 a_1}{\mathrm{d}t^2} = \frac{e^2 k_p^2}{8\omega_1 m_e^2} a_1 (a_{00}^2 + a_{01}^2) + \frac{e^2 k_p^2}{8\omega_1 m_e^2} a_1 a_{00} a_{01}\left[\exp\left(i\Delta\ell\phi\right) + \exp\left(-i\Delta\ell\phi\right)\right]. \tag{6}$$

We now multiply both sides of Eq. (6) by $\exp\left(im\phi\right)$, and integrate both sides along the azimutal direction ϕ. Eq. (6) then leads to:

$$\begin{aligned}\frac{\mathrm{d}^2}{\mathrm{d}t^2}\int a_1 \exp\left(im\phi\right)\mathrm{d}\phi = &\frac{e^2 k_p^2}{8\omega_1 m_e^2}(a_{00}^2 + a_{01}^2)\int a_1 \exp\left(im\phi\right)\mathrm{d}\phi \\ &+ \frac{e^2 k_p^2}{8\omega_1 m_e^2} a_{00}a_{01}\int a_1 \exp\left[i(m+\Delta\ell)\phi\right]\mathrm{d}\phi \\ &+ \frac{e^2 k_p^2}{8\omega_1 m_e^2} a_{00}a_{01}\int a_1 \exp\left[i(m-\Delta\ell)\phi\right]\mathrm{d}\phi.\end{aligned} \tag{7}$$

We now make the following substitutions:

$$\int a_1 \exp\left(im\phi\right)\mathrm{d}\phi \rightarrow f_m \tag{8}$$

$$\int a_1 \exp\left[i(m+\Delta\ell)\phi\right]\mathrm{d}\phi \rightarrow f_{m+\Delta\ell} \tag{9}$$

$$\int a_1 \exp\left[i(m-\Delta\ell)\phi\right]\mathrm{d}\phi \rightarrow f_{m-\Delta\ell} \tag{10}$$

where f_m is the amplitude of the mode with OAM level m. Using these substitutions in Eq. (7), we then arrive to Eq. (3) from the main manuscript:

$$\frac{\mathrm{d}^2 f_m}{\mathrm{d}t^2} = \frac{e^2\omega_p^3}{8m_e^2c^2\omega_1}\left[\left(a_{00}^2+a_{01}^2\right)f_m + a_{00}a_{01}\left(f_{m+\Delta\ell}+f_{m-\Delta\ell}\right)\right], \tag{11}$$

where we have also replaced $k_p = \omega_p/c$.

ANALYTICAL FORMULAS FOR THE AMPLITUDE OF THE OAM HARMONICS

In order to derive explicit analytical formulas for the amplitude of the OAM harmonics we assume that the dominant terms come from the OAM orders that are closer the the initial seed OAM mode. The evolution of the OAM harmonics in the seed laser pulse with initial OAM level ℓ_1, and initially given by $a_{10}\exp\left(i\ell_1\phi\right)$, are then given by:

$$\frac{\mathrm{d}^2 f_{\ell_1\pm\Delta\ell}}{\mathrm{d}t^2} \simeq \frac{e^2\omega_p^3}{8m_e^2c^2\omega_1}(a_{00}^2+a_{01}^2)f_{\ell_1} \tag{12}$$

$$\frac{\mathrm{d}^2 f_{\ell_1\pm\Delta\ell}}{\mathrm{d}t^2} \simeq \frac{e^2\omega_p^3}{8m_e^2c^2\omega_1}a_{00}a_{01}f_{\ell_1\pm(m-1)\Delta\ell} \tag{13}$$

where $m>0$ is a positive integer. We can now recursively solve Eqs. (12) and (13). The solution for the fundamental OAM mode ℓ_1 is:

$$f_{\ell_1} = a_1\cosh\Gamma t, \tag{14}$$

where $\Gamma^2 = (a_{00}^2+a_{01}^2)(e^2\omega_p^3)/(8m_e^2c^2\omega_1)$ is the growth rate. The solution of Eq. (13) for the second OAM harmonic $\ell = \ell_1\pm\Delta\ell$ is:

$$f_{\ell_1\pm\Delta\ell} = \frac{a_{00}a_{01}a_1}{\Gamma^2}\frac{e^2\omega_p^3}{8m_e^2c^2\omega_1}\left[\cosh(\Gamma t)-1\right], \tag{15}$$

where we have used the boundary conditions $f_{\ell_1\pm\Delta\ell}(t=0) = f'_{\ell_1\pm\Delta\ell}(t=0) = 0$. For the third OAM harmonic we have:

$$f_{\ell_1\pm2\Delta\ell} = \frac{a_{00}a_{01}a_1}{\Gamma^2}\frac{e^2\omega_p^3}{8m_e^2c^2\omega_1}\left[\cosh(\Gamma t)-1-\frac{t^2\Gamma^2}{2}\right], \tag{16}$$

and for the fourth OAM harmonic component:

$$f_{\ell_1 \pm 3\Delta\ell} = \frac{a_{00}a_{01}a_1}{\Gamma^2}\frac{e^2\omega_p^3}{8m_e^2c^2\omega_1}\left[\cosh(\Gamma t) - 1 - \frac{t^2\Gamma^2}{2} - \frac{t^4\Gamma^4}{24}\right]. \tag{17}$$

By continuing this procedure we find that the general expression for $f_{\ell_1 \pm m\Delta\ell}$ is thus given by Eq. (4) in the main manuscript:

$$a_1^{\ell_1 \pm |m|\Delta\ell}(t) = a_1\left(\frac{a_{00}a_{01}}{a_{00}^2 + a_{01}^2}\right)^{|m|}\left(\cosh(\Gamma t) - \sum_{i=0}^{|m|-1}\frac{(\Gamma t)^{2i}}{(2i)!}\right). \tag{18}$$

DESCRIPTION OF THE OAM CASCADING MECHANISM

The high orbital angular momentum (OAM) harmonics generation based on stimulated Raman scattering can be interpreted as a cascading process, illustrated schematically in Fig. 1. Figure 1 considers that the pump is composed of two OAM modes, one with $\ell_{00} = 0$ and the other with $\ell_{01} = 1$. The counter-propagating seed is initially composed of a single OAM mode with $\ell_1 = 1$. The initial seed pulse intensity profile is shown on the left hand side of Fig. 1 at $n = 1$ in frame (a)-i. The initial pump and seed k-vector modes in the (k_z, k_ϕ) phase-space are represented in frame (a)-ii. In order to conserve momentum two modes appear in the plasma with $\ell_p = -1$ and $\ell_p = 0$. The new modes are represented by the dashed green vectors in frame (a)-iii. The seed and the new plasma OAM modes are also represented schematically in frame (a)-iv.

In a second step of the cascade (n=2) in Fig. 1 two new modes appear in the seed with $\ell_1 = 0$ and $\ell_1 = 2$, which result from the beating between the plasma modes with $\ell_p = -1$ and $\ell_p = 0$ with the pump modes $\ell_{01} = 1$ and $\ell_{00} = 0$, respectively. The presence of these two new modes changes the seed transverse intensity profile, which becomes asymmetric (frame b-i). In order to conserve momentum, two new additional plasma modes also appear with $\ell_p = -2$ and $\ell_p = +1$.

As the OAM mode cascade progresses, the seed profile becomes further transversely compressed. At the $n = 3$ step of the cascade, two new OAM modes appear with $\ell_1 = -1$ and $\ell_1 = 3$. The seed mode with $\ell_1 = -1$ results from the beating of the pump $\ell_{01} = 1$ with the plasma mode with $\ell_p = -2$. The seed mode with $\ell_1 = 3$ results from the beating of $\ell_{00} = 0$ with the plasma mode $\ell_p = +1$. In turn, conversion of momentum again creates new OAM modes in the plasma with $\ell_p = -3$ and $\ell_p = 2$.

MAXIMUM OAM ORDER PRODUCED BY THE HIGH OAM HARMONICS MECHANISM

This cascaded mechanism continues to create higher OAM harmonics, at least until the breakdown of the paraxial approximation, for which our theoretical model breaks. In the main manuscript we have provided an argument based on the dispersion of the OAM laser. Here, we show that an argument based on the Gouy phase shift can also lead to a similar conclusion.

Consider a Laguerre-Gaussian beam with OAM ℓ and radial index $p = 0$. The Gouy shift is $(|\ell| + 1)\tan^{-1}(z/z_R) \simeq (|\ell| + 1)\lambda_0 z/(\pi w_0^2)$, where z is the propagation distance, $z_R = \pi w_0^2/\lambda_0$ is the Rayleigh length and λ_0 the laser wavelength. Under the paraxial approximation, the Gouy phase shift is smaller than $k_0 z$, where $k_0 = 2\pi/\lambda_0$ is the central laser wavenumber. Thus $2pi\lambda_0 > (|l| + 1)\lambda_0/(\pi w_0^2)$. Defining $r_0 = w_0\sqrt{(\ell/2)}$ as the radius where the OAM beam intensity is maximum, the maximum OAM order $\ell^{\max}$ allowed by the paraxial approximation becomes:

$$\ell^{\max} = \frac{2\pi r_0}{\lambda_0}. \tag{19}$$

The distance between consecutive field maxima at a given propagation distance is $\Delta = 2\pi r_0/\ell$. Hence, according to Eq. (19), the cascade continues as long as the spacing Δ is larger than the laser wavelength, i.e. as long as $\Delta > \lambda_0$. This limit for the maximum topological charge of an OAM laser pulse has also been demonstrated in experiments [6].

SETUP OF NUMERICAL SIMULATIONS AND SIMULATION PARAMETERS

Simulations have been performed using the massively parallel, fully relativistic, electromagnetic particle-in-cell (PIC) code Osiris [3]. In the PIC algorithm, electric currents, electric fields and magnetic fields are defined in a discrete numerical grid. In each grid cell there are simulation particles. Each simulation particle or macro-particle describes the motion of an ensemble of charged particles. The PIC loop has 4 main steps: (i) the motion of each macro-particle is updated using the relativistic Lorentz force equation; (ii) the electric currents are deposited in each grid cell; (iii) electric and magnetic fields are advanced using a finite-difference version of the full set of Maxwell's equations. (iv) the electric and magnetic fields are interpolated back to particles positions. Since the background plasma ion motion

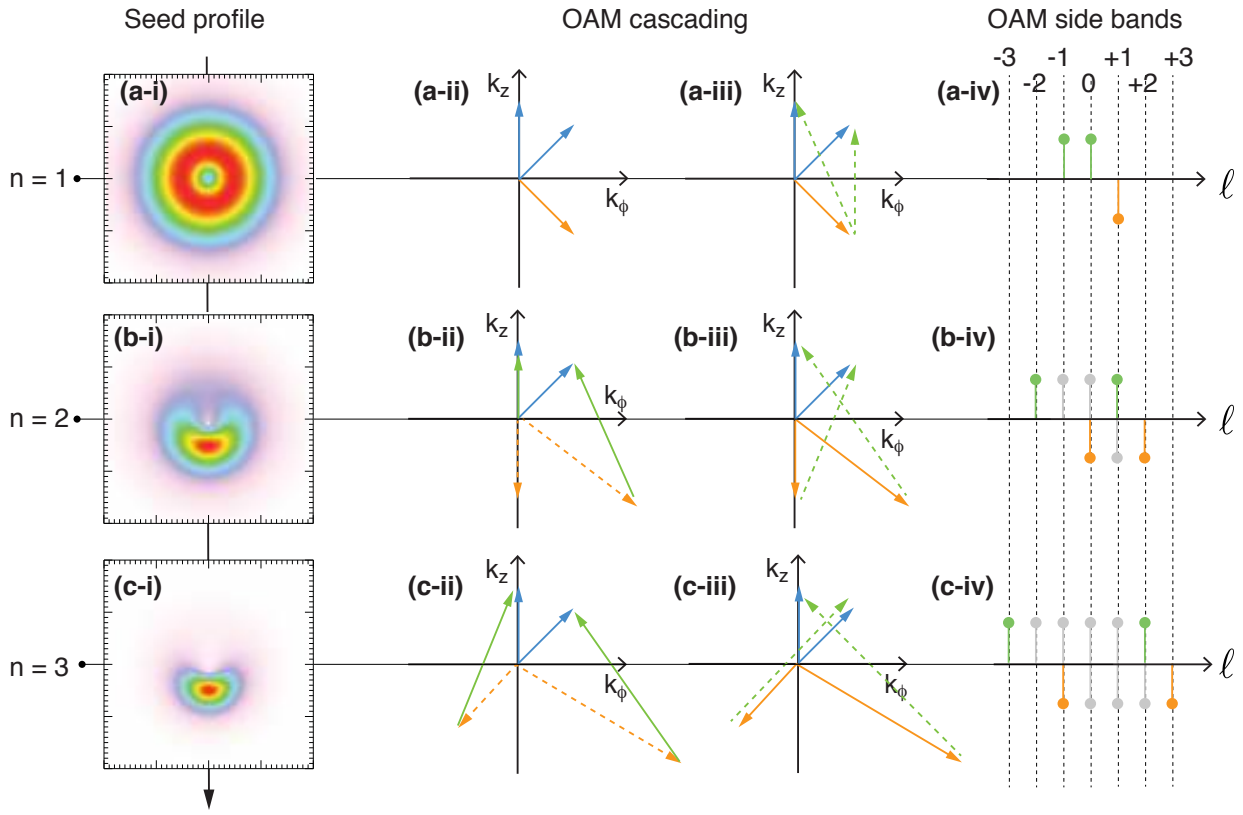

Supplementary Figure 1. Cascading process leading to the generation of the high orbital angular momentum harmonics. Time flows downwards. The evolution of the seed profile is schematically shown in the plots on the left. The middle k-vector diagrams illustrate the creation of the OAM modes in during the first 3 steps in the cascade. The dashed line vectors represent new modes created at a given step. The diagram on the right show the new OAM modes created at each step in colours, and existing modes in grey. Green represents the plasma modes, orange the seed modes, and blue the pump modes. The pump OAM is $\ell_{00} = 0$ and $\ell_{01} = 1$. The initial OAM seed is $\ell_1 = 1$.

is negligible for our conditions, ions have been treated as a positively charged immobile background. The plasma was initialised at the front of the simulation box. In order to save computing time, simulations employ a moving computational window that moves at the speed of light c. The moving window corresponds to a coordinate system that moves at the speed of light c.

The simulation box dimensions are 50 μm $\times$ 2870 μm $\times$ 2870 μm. The simulation box is divided into $650 \times 2400 \times 2400$ cells, where each cell contains $1 \times 1 \times 1$ particles. In total, each

simulation contains 3.7×10^9 simulation particles. The pump laser fields are injected from the leading edge of the moving window [4, 5]. In order to conserve canonical momentum, the initial momentum of each plasma electron macro-particle near the leading edge of the simulation box has been set to match the normalised pump laser vector potential. The particles are initialised with no thermal spread.

The initially linearly polarised OAM seed and pump laser electric fields are given by a superposition of pure Laguerre-Gaussian modes:

$$E = \frac{1}{2}\frac{E_0 w_0}{w(z)}\left(\frac{r\sqrt{2}}{w(z)}\right)^{|\ell|} L_p^{|l|}\left(-\frac{2r^2}{w^2(z)}\right)\exp\left(-\frac{r^2}{w^2(z)}\right) \times \exp\left[ik\left(z-z_0\right)+\frac{ikz}{1+z^2/z_R^2}\frac{r^2}{z_R^2}-i(2p+|\ell|+1)\arctan\left(\frac{z}{Z_r}\right)+i\theta_0+i\ell\phi\right]+c.c \quad (20)$$

where $c.c.$ denotes complex conjugate and where E_0 is the laser electric field at the focus. In addition $w^2(z) = w_0^2\left(1+z^2/Z_r^2\right)$ is the waist of the beam as a function of the propagation distance z in vacuum, w_0 the waist at the focal plane, $Z_r = \pi w_0^2/\lambda$ is the Rayleigh length, $\lambda = 2\pi c/\omega = 2\pi/k$ the central wavelength of the laser, ω and k its central frequency and wavenumber respectively. In addition, $L_p^{|l|}$ is a generalised Laguerre polynomial with order (p, ℓ), with ℓ being the index that gives rise to the orbital angular momentum, $r = \sqrt{x^2+y^2}$ the radial distance to the axis, θ_0 an initial phase, and z_0 the center of the laser. We note that all simulations involving Laguerre-Gaussian modes have $p = 0$.

The wave-number of the pump laser (which travels in the plasma) in all simulations presented is set according to the linear plasma dispersion relation $k^2c^2 = \omega^2 - \omega_{\rm p}^2$, where $\omega_{\rm p} = \sqrt{4\pi n_0 e^2/m_e}$ is the plasma frequency associated with a background plasma density n_0, and where e and m_e are, respectively, the elementary charge and electron mass. The seed frequency and wavenumber are set according to the matching conditions for Raman amplification (see Table 1).

The parameters of the seed and pump for each 3D simulation are shown in Table .

NUMERICAL FOURIER ANALYSIS OF PIC SIMULATIONS

The amplitude, $E_L(\varphi)$ of a laser field E_L can be generally written as:

$$E_L(\varphi) = \sum_{|\ell|=0}^{\infty} E_\ell(\varphi, \pm|\ell|), \quad (21)$$

Figures	**3a-b, 4a**		**3c-d, 4b**		**4c**		**4d**	
	Pump	**Seed**	**Pump**	**Seed**	**Pump**	**Seed**	**Pump**	**Seed**
OAM	$\Delta\ell = 1$	$\ell_1 = 0$	$\Delta\ell = 2$	$\ell_1 = 0$, $\ell_1 = 1$	$\Delta\ell = 4$	$\ell_1 = 1$	$\Delta\ell = 6$	$\ell_1 = -1$
$\mathbf{a_0}[\times\mathbf{10^{-2}}]$ **(peak)**	(1.8, 2.2)	3.5	(1.5,2.2)	3.5	(2.2,2.2)	1.4	(5.4,2.2)	1.5
spot (μ**m**)	435	717	435	717	384	384	(384,665)	538
duration (**fs**)	25×10^3	25	25×10^3	25	25×10^3	25	25×10^3	25
$\boldsymbol{\omega_0/\omega_p}$	20	19	20	19	20	19	20	19

TABLE I. **Initial seed and pump laser parameters used for the high OAM harmonic generation simulations**. The central wavelength of the seed pulse in all simulations is 1 μm. The background plasma density in all simulations is $n_0 = 4.3 \times 10^{18}\text{cm}^{-3}$. The peak pump laser a_0 is represented as (a_{00}, a_{01}), where a_{00} and a_{01} are the peak a_0 values for each pump mode.

where $\varphi = \omega_0 t - k_0 z$ is the phase, and $\pm\ell$ is the OAM. Each mode E_ℓ is given by:

$$E_\ell(\varphi, \pm\ell) = A_{+|\ell|}\cos(\varphi + \ell\theta) + A_{-|\ell|}\cos(\varphi - \ell\theta) + B_{+|\ell|}\sin(\varphi + \ell\theta) + B_{-|\ell|}\sin(\varphi - \ell\theta)\,. \tag{22}$$

The amplitude of a mode with $+|\ell|$ is given by $\sqrt{A^2_{+|\ell|} + B^2_{+|\ell|}}$ and the amplitude of a mode with $-|\ell|$ is $\sqrt{A^2_{-|\ell|} + B^2_{-|\ell|}}$. In order to find the coefficients $A_{\pm\ell}$ and $B_{\pm\ell}$ we solve the following 4 independent linear equations:

$$I_{+|\ell|} = \int_0^{2\pi} E_L(\varphi_1)\sin(\ell\theta)\,\mathrm{d}\theta = \int_0^{2\pi} E_\ell(\varphi_1)\sin(\ell\theta)\,\mathrm{d}\theta \tag{23}$$

$$I_{-|\ell|} = \int_0^{2\pi} E_L(\varphi_1)\sin(-\ell\theta)\,\mathrm{d}\theta = \int_0^{2\pi} E_\ell(\varphi_1)\sin(-\ell\theta)\,\mathrm{d}\theta \tag{24}$$

$$J_{+|\ell|} = \int_0^{2\pi} E_L(\varphi_2)\cos(\ell\theta)\,\mathrm{d}\theta = \int_0^{2\pi} E_\ell(\varphi_2)\cos(\ell\theta)\,\mathrm{d}\theta \tag{25}$$

$$J_{-|\ell|} = \int_0^{2\pi} E_L(\varphi_2)\cos(-\ell\theta)\,\mathrm{d}\theta = \int_0^{2\pi} E_\ell(\varphi_2)\cos(\ell\theta)\,\mathrm{d}\theta, \tag{26}$$

where φ_1 and φ_2 are two phases, and where $I_{\pm|\ell|}$ and $J_{\pm|\ell|}$ are given by the numerical integration of the laser field retrieved from the simulations. Equation 23 is solved for every transverse simulation slice. The results in Fig. 4 are then retrieved at a particular simulation longitudinal position.

[1] D.W. Forslund, J.M. Kindel, E.L. Lindman, Phys. Fluis **18**, 1002 (1975).

[2] J. Vieira *et al.*, Nature Comms. (accepted, 2016).

[3] R. A. Fonseca *et al.*, Plasma Phys. Control. Fusion **55**, 124011 (2013).

[4] P. Mardahl *et al.*, XOOPIC Simulations of Raman Backscattering, Bull. Am. Phys. Soc. **46**, DPP 2001, KP1.108 (2001)

[5] P. Mardahl, PIC Code Charge Conservation, Numerical Heating, and Parallelization: Application of XOOPIC to Laser Amplification via Raman Backscatter, Ph.D. thesis, University of California, Berkeley (2001)

[6] R. Zambrini, L. C. Thomson, S. M. Barnett, M. Padgett, Journal Mod. Optics **58**, 1135 (2005).